

# Phase Behavior of Highly Immiscible Polymer Blends Stabilized by a Balanced Block Copolymer Surfactant

Joon H. Lee,<sup>†</sup> Megan L. Ruegg,<sup>†</sup> Nitash P. Balsara,<sup>\*,†,‡</sup> Yuqing Zhu,<sup>§</sup>  
Samuel P. Gido,<sup>§</sup> Ramanan Krishnamoorti,<sup>⊥</sup> and Man-Ho Kim<sup>#</sup>

Department of Chemical Engineering, University of California, Berkeley, California 94720; Materials Sciences Division, Lawrence Berkeley National Laboratory, Berkeley, California 94720; Department of Department of Polymer Science and Engineering, University of Massachusetts, Amherst, Massachusetts 01003; Department of Chemical Engineering, University of Houston, Houston, Texas 77204; Center for High-Resolution Neutron Scattering, National Institute of Standards and Technology, Building E235, Gaithersburg, Maryland 20899; and Department of Materials and Nuclear Engineering, University of Maryland, College Park, Maryland 20742

Received January 9, 2003; Revised Manuscript Received April 23, 2003

**ABSTRACT:** The phase behavior of mixtures of polyisobutylene (PIB), polyethylene (PE), and a symmetric polyethylene-*block*-head-to-head polypropylene copolymer (PE-PP) was studied by transmission electron microscopy (TEM) and small-angle neutron and light scattering. The thermodynamic interactions between PE/PP and PE/PIB are repulsive (Flory-Huggins parameter  $\chi > 0$  and decreases with increasing temperature), while those between PP/PIB are attractive ( $\chi < 0$  and increases with increasing temperature). When the PE-PP copolymer is added to a 50/50 PE/PIB mixture, the resulting phase diagram in temperature-copolymer composition space exhibits many of the characteristics of “fish-shaped” phase diagrams found in oil/water mixtures stabilized by balanced surfactants. This is due to the interplay between the different  $\chi$  parameters that characterize the system. Lamellar phases, single droplet microemulsions, and bicontinuous microemulsions were observed. The length scales of these structures and the locations of the phase transition points on the phase diagram determined by TEM and scattering are in reasonable agreement. Phase transitions from a lamellar phase to a single droplet microemulsion phase, and from a bicontinuous microemulsion to a macrophase-separated structure, have been identified.

## Introduction

The word surfactant usually refers to a molecule that is used to modify the interfacial properties of aqueous systems. In their presence, mixtures of oil and water self-organize into a variety of structures such as vesicles, bilayers, lamellae, and microemulsions.<sup>1–3</sup> This rich phase behavior is due to the availability of different types of surface-active molecules such as ionic and nonionic surfactants, cosurfactants, phospholipids, proteins, etc. These molecules were obtained either by human trial-and-error or by evolution. Our objective is to use surfactant design concepts established in aqueous systems to create a library of surfactants for organizing other immiscible fluids. The concept that we focus on in this paper is that of *balance*.

Oil/water mixtures are unique because hydrophilic moieties are usually oil-phobic and hydrophobic moieties are usually oil-philic. The behavior of surfactants for these systems is thus governed by two characteristics: hydrophilicity and hydrophobicity. In contrast, surfactants for mixtures of two arbitrary fluids, A and B, will be governed by four independent characteristics: A-philicity and A-phobicity, B-philicity and B-phobicity. A-philicity does not necessarily imply B-phobicity, and A-phobicity does not necessarily imply B-philicity.

This paper deals with the problem of designing surfactants for highly immiscible polymers. Our objec-

tive is to obtain single-phase, microphase-separated states in these systems. Numerous papers have been written on the potential use of A-B block and graft copolymers for controlling the interface between A and B homopolymers.<sup>4–32</sup> The logic for this choice of polymeric surfactants is simple. It is believed that the A-block gives the surfactant A-philic character while the B-block gives the surfactant B-philic character. This choice of surfactants, however, does not enable *independent* control over the four characteristics that were identified in the preceding paragraph. This is because the thermodynamics of A/B/A-B mixtures are controlled by a single interaction: that between A and B chains (in polymer systems one usually uses the Flory-Huggins parameter,  $\chi$ , to characterize these interactions).

Pioneering studies by Bates, Lodge, and co-workers have demonstrated the ability of A-B block copolymers to stabilize the interface between nearly miscible A/B blends.<sup>4–8</sup> It is now recognized, however, that A-B block copolymers cannot serve as surfactants for highly immiscible homopolymers A and B. Theoretical calculations<sup>23,24,27,28</sup> show that as the incompatibility between the homopolymers increases, the ternary phase diagram changes qualitatively, and a large unorganized three-phase window consisting of two homopolymer-rich phases and one copolymer rich phase is obtained. While the formation of separate copolymer-rich phases in A/B/A-B mixtures has been reported several times in the literature (e.g., ref 8), systematic experiments that confirm the presence of the theoretically predicted three-phase window are given in ref 7. There is thus clearly

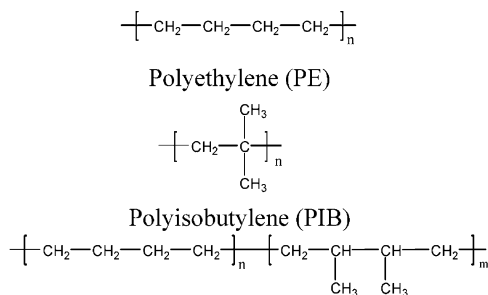
<sup>†</sup> University of California, Berkeley.

<sup>‡</sup> Lawrence Berkeley National Laboratory.

<sup>§</sup> University of Massachusetts.

<sup>⊥</sup> University of Houston.

<sup>#</sup> National Institute of Standards and Technology and University of Maryland.



Polyethylene-*block*-head-to-head polypropylene (PE-PP)

**Figure 1.** Chemical structure of the components used in this study: polyethylene, polyisobutylene, and polyethylene-*block*-head-to-head polypropylene copolymer.

**Table 1.** Nomenclature for A/B/A-C Systems

| component | aqueous system         | polymer system             |
|-----------|------------------------|----------------------------|
| A         | alkane                 | polyethylene               |
| B         | water                  | polyisobutylene            |
| A-C       | alkyl polyglycol ether | polyethylene-polypropylene |

a need to develop other complementary strategies for stabilizing interfaces between immiscible polymers.

Alkyl polyglycol ether molecules (often referred to as nonionic or  $C_iE_j$  surfactants) are examples of effective surfactants for oil/water mixtures. Single-phase, microphase-separated states are obtained in these systems despite the extremely low mutual solubility of oil and water. The hydrophobic and hydrophilic interactions of these nonionic surfactant molecules are comparable in magnitude.<sup>33-39</sup> They are thus often referred to as balanced surfactants. Our objective is to study the phase behavior of mixtures of highly immiscible polymers—polyethylene (PE) and polyisobutylene (PIB)—in the presence of a balanced surfactant. The surfactant that we have chosen for this study is a polyethylene-*block*-head-to-head polypropylene diblock copolymer (PE-PP). The chemical structures of the components used here are shown in Figure 1. Our conclusions are based on a combination of small- and ultrasmall-angle neutron scattering, polarized and depolarized small-angle light scattering, and transmission electron microscopy. The present work lends considerable support to conclusions based on preliminary data given in ref 40.

### Phenomenology of Balanced Surfactants

The term “A/B/A-C” mixtures could be used to describe both aqueous systems and our polymer blend: A is either alkane or PE, B is either water or PIB, and C is either the polyglycol ether or PP. For convenience, our definitions of A, B, and C are summarized in Table 1. The phase diagram obtained when a balanced A-C surfactant is added to a 50/50 A/B mixture in temperature-surfactant volume fraction ( $T-\phi_{A-C}$ ) space has the shape of a fish and is shown schematically in Figure 2.<sup>33,41</sup> Below a certain surfactant volume fraction, denoted by  $\phi_1$  in Figure 2, the surfactant has little effect on a phase-separated oil/water mixture, and two coexisting oil-rich and water-rich phases are obtained. When  $\phi$  is between  $\phi_1$  and  $\phi_2$ , oil-rich and water-rich phases coexist with a third surfactant-rich phase. This three-phase window forms the head of the fish. When  $\phi$  is greater than  $\phi_2$ , single-phase systems are obtained within a temperature range that widens with increasing surfactant concentration. This single-phase window, which forms the tail of the fish in Figure 2, is composed of three distinct regions. Lamellae are formed in the

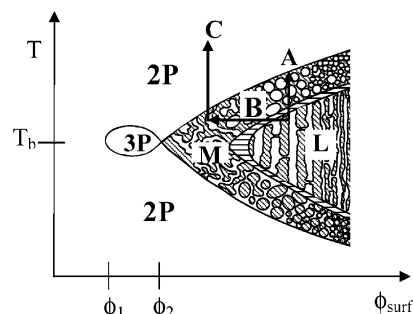


**Figure 2.** Schematic of the phase diagram of an A/B/A-C mixture in  $T-\phi_{A-C}$  space along the  $\phi_A = \phi_B$  isopleth, when the A-C surfactant is balanced.  $\phi_i$  is the volume fraction of species  $i$ . The notation for the various phases is as follows: 3P, three coexisting phases; 2P, two coexisting phases; M, microemulsion; L, lamellae. Region of coexistence of L and M phases appears between the L and M regions. Arrows labeled A, B, and C indicate the phase transitions studied in this paper.

middle of the tail while microemulsions are formed toward the edge of the tail. A region of coexistence separates the lamellar and microemulsion regions. Bicontinuous microemulsions are obtained near the head-tail junction ( $\phi \approx \phi_2$ ), while droplet microemulsions are obtained farther away from the head ( $\phi > \phi_2$ ). All of the phases described above form in a temperature window centered<sup>41</sup> about  $T_b$ , the balance temperature, as shown in Figure 2.

Our PE/PIB/PE-PP blend is symmetric in many respects. The volume fractions and molecular volumes of the PE and PIB homopolymers are equal (or nearly so), and the PE-PP copolymer is symmetric ( $f_{PE}$ , the volume fraction of the PE block in the copolymer, is about 0.5). Because of this symmetry, the curvature of the interface between A-rich and B-rich domains is determined entirely by surfactant-homopolymer interactions.

The temperature dependence of the Flory-Huggins interaction parameter for PE/PP and PIB/PP homopolymer mixtures is given by<sup>42-44</sup>

$$\chi_{AC} = \chi_{PE/PP} = -0.018 + 11.0/T \quad (1)$$

and

$$\chi_{BC} = \chi_{PIB/PP} = 0.018 - 7.7/T \quad (2)$$

where  $T$  is in K and  $\chi$  is based on a reference volume of  $100 \text{ \AA}^3$ . Note that the coefficients which determine the temperature dependence of  $\chi_{AC}$  and  $\chi_{BC}$  are opposite in sign.  $\chi_{AB}$  ( $\chi_{PE/PIB}$ ) has not yet been measured due to the extreme incompatibility of PE and PIB.<sup>45</sup>

The incompatibility between A and B will lead to the formation of A-rich and B-rich phases that are almost pure, and we refer to these phases as the A-phase and B-phase, respectively. For simplicity, we assume the presence of a monolayer of the A-C copolymer molecules at the interface between the A- and B-phases.<sup>46</sup> It is clear that such a monolayer is essential for obtaining the phase behavior seen in Figure 2. The strong repulsion between A and B will force the A-block away from the B phase. (Throughout this paper, we will use “A” to denote the homopolymer chain and “A-block” to denote the A chain that is part of the A-C block copolymer.) The C-block is thus forced to reside in the B-phase. This tendency is reinforced by the fact that  $\chi_{BC}$  is negative (i.e., B/C interactions are attractive) over a substantial range of temperatures (see eq 2). In

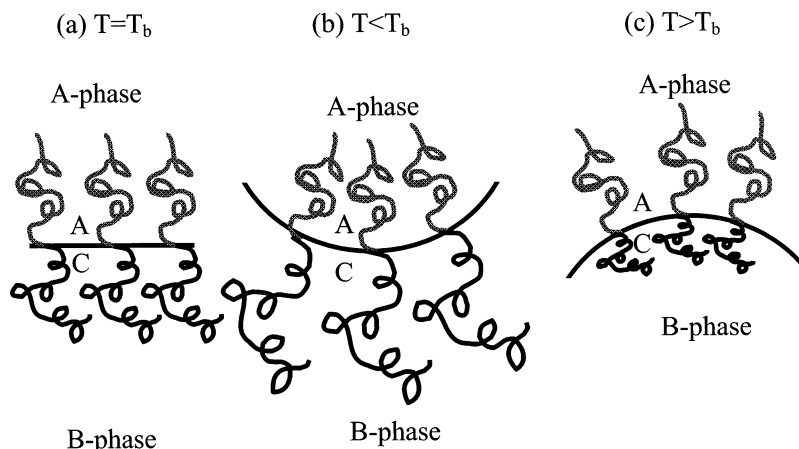


**Figure 3.** Chain conformation of the A–C block copolymer molecules when they lie at the interface between A-rich and B-rich phases and the resulting curvature of the interface. (a) At the balance temperature  $T = T_b$ , interfaces with zero mean curvature are formed due to balanced A–A and C–B interactions. (b) At  $T < T_b$ , attractive C–B interactions lead to swelling of the C-block. (c) At  $T > T_b$ , repulsive C–B interactions lead to collapse of the C-block.

contrast,  $\chi_{AC}$  is positive over the entire temperature range of interest (see eq 1). We thus expect the A-block to contact the A-phase and the C-block to contact the B-phase. The expected orientation of an A–C molecule located at a flat interface between the A-phase and the B-phase is given in Figure 3a.

Theories on interfaces bearing block copolymers suggest that the curvature of these interfaces is governed by the swelling of the blocks.<sup>26</sup> The interactions between a brush of A-blocks with an A homopolymer melt are entropic in origin (all chain conformations have the same energy), and they depend on the molecular weight of the free chains relative to those comprising the brush.<sup>47</sup> We expect the swelling of the A-block to be temperature-independent. The temperature dependence of the curvature of the interface is thus governed by the swelling of the C-block in the B-rich phase, which in turn depends on the temperature dependence of  $\chi_{BC}$ .

Near the balance temperature,  $T_b$ , the phases that appear in the one-phase window are lamellae and bicontinuous microemulsions, which contain interfaces with zero mean curvature. We thus expect that at  $T = T_b$  the degree of swelling of the A-block in contact with the A-phase is similar to that of the C-block in contact with the B-phase. This is shown schematically in Figure 3a. Because  $\chi_{AA}$  is zero at all temperatures (by definition of  $\chi$ ), one expects the C-block in the B-phase to assume similar conformations as the A-block in the A-phase at the temperature at which  $\chi_{BC} \approx 0$ . This suggests that the balance temperature,  $T_b$ , is approximately given by  $\chi_{BC}(T_b) = 0$ , i.e.,  $T_b \approx 155$  °C (eq 2). At the balance temperature, the A-philic and B-philic tendencies of the A–C block copolymer are equal.

At temperatures below  $T_b$ ,  $\chi_{BC}$  is negative (eq 2). The C-block will thus be in a swollen state (relative to the A-block). Simple geometric arguments<sup>26,48</sup> would then place the C-block on the outside of the curved interface, as shown schematically in Figure 3b. At temperatures above  $T_b$ ,  $\chi_{BC}$  is positive (eq 2). The C-block will be in a collapsed state, which in turn will lead to the placement of the C-block on the inside of the curved interface. This is shown schematically in Figure 3c. We thus expect the lamellar phase to give way to A-droplets at low temperatures and B-droplets at high temperatures, as shown in Figure 2. The transition temperature from lamellae to droplets for a given surfactant concentration will be obtained when the conformational entropy

gained by the outer block is sufficient to overcome the increase in free energy due to a variety of contributions such as curvature elasticity, interfacial energy, and decrease in entropy of the inner block. These factors will be governed mainly by  $\chi_{AC}$ ,  $\chi_{AB}$ , and  $\chi_{BC}$ . These three independent parameters enable significant control over the four important characteristics of the surfactant molecule, namely A-philicity and A-phobicity, B-philicity and B-phobicity. In the absence of a theoretical framework for quantifying the relationships between binary interaction parameters and multicomponent behavior, we chose the chemical composition of the C-block such that the temperature dependencies of  $\chi_{AC}$  and  $\chi_{BC}$  would be similar in magnitude and opposite in sign (see eqs 1 and 2). We assumed that this would lead to a phase diagram that was symmetric about  $T_b$ , as shown in Figure 2. The molecular weight of the A–C block copolymer was chosen such that the order–disorder transition of the neat copolymer was in the vicinity of  $T_b$ . The PE–PP block copolymer used here was also used in ref 13 where we determined that the order–disorder transition temperature of the PE–PP block copolymer is  $149 \pm 2$  °C.

The arguments given here are simplistic. The conformation of the A–C diblock will undoubtedly depend on other factors such as concentration fluctuations, interfacial excess of the block copolymer (brush density), the statistical segment lengths of the chains, etc. It thus is unlikely that  $T_b$  will be governed solely by  $\chi_{BC}$ , as indicated above. The qualitative arguments given above are meant to serve as a starting point for understanding the phase behavior described in Figure 2. We note in passing that there is considerable recent interest in the thermodynamics of polymer blends wherein both attractive and repulsive interactions are present.<sup>49–55</sup>

The experiments described below provide evidence for the existence of some of the phase transitions described above in PE/PIB/PE–PP blends. The particular phase transitions addressed in this paper are indicated by arrows labeled A, B, and C in Figure 2.

### Experimental Details

Fully hydrogenous and partially deuterated polyolefins, polyethylene (PE) and poly(ethylene-*block*-head-to-head propylene) (PE–PP), were synthesized by anionic polymerization of dienes followed by saturation of the double bonds with hydrogen or deuterium.<sup>13</sup> All reagents were purified using

standard high-vacuum techniques. The PIB sample was synthesized by cationic polymerization.<sup>56</sup> The empirical formula of all of the components, including the surfactant, is CH<sub>2</sub>. The weight-averaged molecular weights of the components  $M_i$  were determined to be  $M_{PE} = 12$  kg/mol,  $M_{PIB} = 14$  kg/mol, and  $M_{PE-PP} = 66$  kg/mol, and the volume fraction of PE in PE-PP is 0.49. The average hydrogen-to-deuterium atom ratio in the PE chains was 2.2, while those in the PE-block and PP-block of the copolymer were 1.1 and 2.1, respectively. The polydispersity index of all of the polymers was 1.1 or less. Our characterization procedures are described in ref 21. Multicomponent PE/PIB/PE-PP blends were prepared by methods described in ref 13. The ratio of the volume fractions of the homopolymers,  $\phi_{PE}/\phi_{PIB}$ , was fixed at 1.05 for all blends (approximately the critical composition of the binary homopolymer blend). We prepared four blend samples containing 10, 15, 20, and 30 vol % block copolymer, labeled B10, B15, B20, and B30, respectively. Small-angle neutron and light scattering experiments were conducted on 1 mm thick blend samples encased between quartz windows.

Small-angle neutron scattering (SANS) experiments were conducted on the NG3 beamline at the National Institute of Standards and Technology (NIST) in Gaithersburg, MD. Instrumental details and data reduction procedures are similar to those in refs 13 and 42 and are given in ref 57. We report the azimuthally averaged scattering intensity,  $I$ , as a function of  $q$  [ $q = 4\pi \sin(\theta/2)/\lambda$ ,  $\theta$  is the scattering angle,  $\lambda$  is the wavelength of the incident beam (1.2 nm for SANS)], in the temperature range between 113 °C (slightly above the crystallization temperature of the PE chains) and 194 °C (the upper limit of the SANS sample holder). The sample temperature was controlled to  $\pm 1$  °C.

Sample B10 (encased between quartz windows) was studied by ultrahigh-resolution small-angle neutron scattering (USANS) at the thermal neutron port BT5 at NIST in Gaithersburg, MD. Details regarding instrumentation and data analysis are given in ref 66. We used a Bonse-Hart type perfect-crystal diffractometer, equipped with triple bounce channel-cut perfect Si (220) crystals as the monochromator and the analyzer. The incident neutron beam with wavelength  $\lambda = 0.24$  nm was collimated using a 12.7 mm diameter aperture. A 0.3 mm thick B10 sample was placed in a preheated sample stage at  $143 \pm 2$  °C between the monochromator and analyzer. Data acquisition was started 3 h after placing the sample in the heating stage to ensure equilibration. The collected data were normalized with the monitor count rate and then converted in absolute intensity ( $\text{cm}^{-1}$ ) after correcting for sample transmission (75% for this sample) and background scattering. The data reduction described above was carried out using the USANS data reduction program at NIST. The reduced scattering profiles were corrected for detector smearing using a program written by John Barker to give the USANS intensity,  $I$ , vs scattering vector,  $q$ .

Small-angle light scattering experiments were conducted with a 10 mW HeNe laser, with wavelength  $\lambda_{\text{light}} = 633$  nm, directed through samples placed in a temperature-controlled heating unit. The scattered light was focused on a detector, in the range of  $4.33 \times 10^{-4} \text{ nm}^{-1} < q < 1.85 \times 10^{-3} \text{ nm}^{-1}$ , using a beam stop and a focusing lens. (The definition of  $q$  given above in our discussion of SANS experimental details holds for both light and neutron scattering.) The instrumental details are given in ref 57. Depolarized small-angle light scattering (DSALS) measurements were made on the same instrument with the addition of a second polarizer (the analyzer) placed after the sample with its polarization direction perpendicular to the incident polarization. Without the use of the beam stop the range of accessible scattering vectors in this configuration was  $0 \text{ nm}^{-1} < q < 1.85 \times 10^{-3} \text{ nm}^{-1}$ . Both SALS and DSALS intensities,  $I_{\text{SALS}}$  and  $I_{\text{DSALS}}$ , respectively, were monitored as a function of time after the sample was heated in a stepwise manner from one predetermined temperature to another. The upper limit of the light scattering sample holder was 250 °C.

Blends B10, B15, and B20 were examined by TEM. The TEM samples were encased in glass tubes and annealed under vacuum for a minimum of 2 h at a predetermined temperature

(either 145 or 160 °C) and then rapidly quenched by immersion in liquid nitrogen in order to freeze the microstructure at the experimental temperature. On the basis of the thermal properties of polyolefins, we expect the center of the sample to reach 100 °C (below the crystallization temperature of PE) in about 10 s. To ensure complete freezing, the samples were kept at liquid nitrogen temperatures for about 30 min. Ultrathin sections (about 50 nm thick) were obtained using a Leica cryoultramicrotome at  $-120$  °C. The sections were stained by RuO<sub>4</sub> and examined by a JEOL 100CX transmission electron microscope operating at 100 kV.

The attractive feature of electron microscopy is the ability to observe the structure of the sample directly in position space. However, there are two factors that must be taken into consideration when analyzing the images obtained from our multicomponent samples:

(1) The ability of different phases to absorb the staining compound depends on the chemical interactions between RuO<sub>4</sub> (our staining compound) and the components of the phases. RuO<sub>4</sub> attacks polyolefins by oxidation of C-H bonds.<sup>58</sup> Components with H atoms attached to tertiary C atoms are thus most susceptible to attack. The concentration of such H atoms is much larger in PP than in PE (Figure 1). There are no H atoms attached to tertiary C atoms in PIB. The extent of staining is also affected by the diffusivity of RuO<sub>4</sub> through the phases in the sample.<sup>59</sup> We expect rapid diffusion of RuO<sub>4</sub> through PP because it is amorphous, and we expect slower diffusion through PE because it is semicrystalline. The impermeability of low molecular weight compounds like RuO<sub>4</sub> through PIB is well established<sup>60-62</sup> and is the basis of many applications of PIB.<sup>63</sup> Arguments based on both chemical interactions and diffusivity thus lead to the following assignments: the PIB-rich phase is bright (least stained), the PP-rich phase is dark (most stained), and the PE-rich phase will absorb an intermediate amount of the staining compound.

(2) The microstructure observed in TEM is that from a quenched sample. It is possible that the microstructure at the elevated temperatures is distorted by the quenching process. Our goal was to freeze the PE chains with minimal disruption of the structure in the molten state. In pure block copolymers containing crystalline and amorphous blocks, it has been shown that distortion due to crystal formation is a complex function of quenching conditions, block copolymer architecture, and the symmetry of the phase that one wishes to preserve.<sup>64,65</sup> Similar studies on complex multicomponent mixtures have not yet been conducted. The extent to which the present protocol disrupts the melt structure in our A/B/A-C mixtures is thus an open question.

## Results and Discussion

The SANS intensity profiles,  $I(q)$ , obtained from B20 at selected temperatures are shown in Figure 4a. At 145 °C we see a primary scattering peak centered at  $q_1 = 0.07 \text{ nm}^{-1}$  and a secondary scattering peak centered at  $q_2 = 0.14 \text{ nm}^{-1}$ , corresponding to the first- and second-order peaks of the lamellar phase with characteristic length  $d = 2\pi/q_1 = 90$  nm. At 160 and 179 °C, we see a broad primary peak with little or no evidence of a secondary peak (Figure 4a). These scattering profiles are qualitatively consistent with that expected from both droplet and bicontinuous microemulsions.<sup>39</sup> At 194 °C, we observe a sharp increase in the low-angle SANS ( $0.02 \text{ nm}^{-1} \leq q \leq 0.04 \text{ nm}^{-1}$ ), and the primary scattering peak is reduced to a shoulder (Figure 4a). This indicates that the periodic structure obtained at the lower temperatures is lost at 194 °C. The SANS profiles from B15, shown in Figure 4b, are qualitatively similar to those seen in Figure 4a. At 145 °C we see two peaks at  $q_1 = 0.05 \text{ nm}^{-1}$  and  $q_2 = 0.11 \text{ nm}^{-1}$ , indicating the presence of a lamellar phase with  $d = 120$  nm. At 160 °C we see the scattering signature of microemulsions, and at 179 °C we see a sharp increase in the low-angle scattering

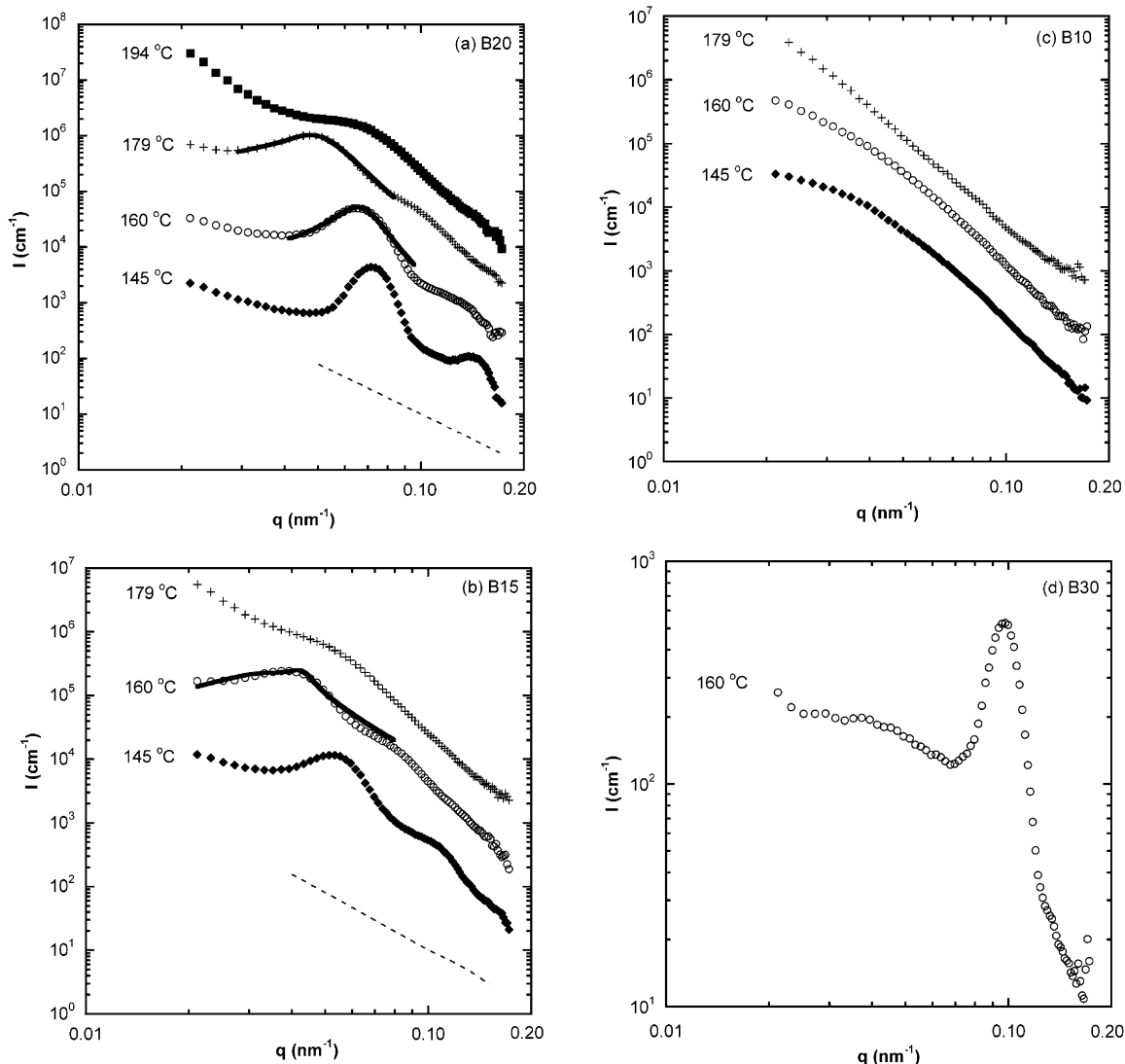


**Figure 4.** SANS profiles from PE/PIB/PE-PP blends at selected temperatures with (a) 20% PE-PP, (b) 15% PE-PP, (c) 10% PE-PP, and (d) 30% PE-PP.<sup>77</sup>  $I(q)$  at 160, 179, and 194 °C have been multiplied by factors of 10, 100, and 1000, respectively, to increase the clarity of the plots. The data at 160 and 179 °C for B20 (a) and at 160 °C for B15 (b) have been fit to the Teubner-Strey equation [ $I = 1/(a + bq^2 + cq^4) + 1/(dq^2 + eq + f)$ ]. The values obtained for B20 at 160 °C were  $a = 0.00163$ ,  $b = -0.677$ ,  $c = 79.5$ ,  $d = 6236.1$ ,  $e = -143.2$ ,  $f = -18.7$ , and those at 179 °C were  $a = 0.000261$ ,  $b = -0.170$ ,  $c = 39.1$ ,  $d = -1.52$ ,  $e = 0.132$ ,  $f = -0.00316$ . The values obtained for B15 at 160 °C were  $a = 0.000169$ ,  $b = -0.165$ ,  $c = 54.50$ ,  $d = 0.568$ ,  $e = -0.0147$ ,  $f = 0.000192$ . The units of the fit parameters are such that  $I$  is expressed in  $\text{cm}^{-1}$  and  $q$  is expressed in  $\text{nm}^{-1}$ . The fit parameters were obtained on the measured (unshifted)  $I$  vs  $q$  data.

and the primary scattering peak is reduced to a shoulder. It is worth noting that the scattering peaks observed in samples B20 and B15 are superposed on a “background” that is highly  $q$ -dependent. For the case of sample B15 at 145 °C, for example,  $I(q)$  at the primary peak and  $I(q)$  at the lowest accessible  $q$  ( $q = 0.02 \text{ nm}^{-1}$ ) are comparable in magnitude. If we approximate this background by a power law scattering function [ $I(q) \sim q^{-x}$ ], then the exponent that approximately matches the background scattering function is  $x = 3$ . The dashed curves in Figure 4a,b represent  $q^{-3}$  power laws.

Typical  $I(q)$  data obtained from B10 are shown in Figure 4c. The absence of clearly resolved scattering peaks from B10 indicates that either the blend does not contain a periodic microstructure in the temperature range of interest, or the characteristic length ( $d$ ) of the microstructure is outside the resolution limit of the SANS instrument, i.e.,  $d$  is greater than 300 nm in the temperature range of the experiments. At 160 °C, however, we obtain a single power law, and to a good

approximation,  $I \sim q^{-4}$  over the entire accessible  $q$  range. This is an indication of a macrophase-separated sample wherein Porod scattering from the interfaces between the macrophases dominates the measured scattering profiles.

B30 showed a primary peak in the accessible  $q$ -window at all temperatures. Typical  $I(q)$  data obtained from B30 are shown in Figure 4d where we see a primary peak at  $q \approx 0.09 \text{ nm}^{-1}$ . No qualitative changes in the peak width or position were seen in the accessible temperature window.

The scattering from microemulsions in the vicinity of the primary maximum is often described by the Teubner-Strey equation:<sup>39</sup>

$$I(q) = 1/(a + bq^2 + cq^4) + I_{\text{bgd}}(q) \quad (3)$$

where  $a$ ,  $b$ , and  $c$  are  $q$ -independent constants. The scattering from polymer microemulsions contains con-

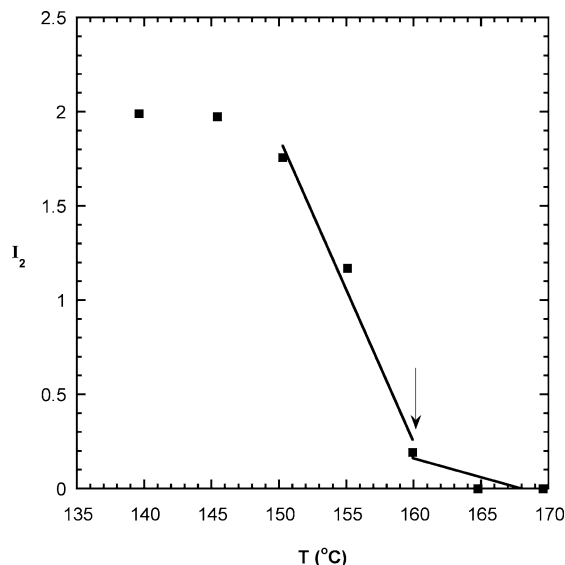


**Figure 5.** Area under the second-order peak ( $I_2$ ) vs temperature is shown for B20. The lamellae-to-microemulsion transition occurs at  $T \approx 160$  °C (arrow), the temperature step that results in  $I_2$  approaching zero. A two-line linear least-squares fit<sup>78</sup> was used to determine the transition temperature.

**Table 2. Microemulsion Correlation Length and Domain Spacing**

|                                | B20<br>(160 °C) | B20<br>(179 °C) | B15<br>(160 °C) |
|--------------------------------|-----------------|-----------------|-----------------|
| correlation length, $\xi$ (nm) | 85              | 70              | 90              |
| domain spacing, $d$ (nm)       | 95              | 129             | 155             |

tributions due to effects such as chain connectivity, and these factors are lumped into the background term  $I_{bgd}(q)$ . We assume that  $1/I_{bgd}(q)$  is a quadratic function:  $I_{bgd}(q) = 1/(eq^2 + fq + g)$ .<sup>40,67</sup> The curves in Figure 4a are least-squares fits of eq 3 through the SANS data from B20 in the neighborhood of the primary peak obtained at 160 and 179 °C, with  $a-g$  as adjustable parameters. The agreement between the measured scattering profiles and the Teubner–Strey equation suggests that B20 is a microemulsion at these temperatures. Similar analysis was conducted on the data obtained from B15 at 160 °C (Figure 4b).

The Teubner–Strey scattering function is based on a correlation function  $C(r) = (e^{-r/\xi}/r) \sin(2\pi r/d)$ , where  $d$  is the average interdomain spacing and  $\xi$  is the correlation length. The values of  $d$  and  $\xi$  obtained using eq 9 and 10 in ref 39 for our microemulsions are given in Table 2. As expected, the correlation lengths are smaller than the average interdomain spacing in all of the microemulsions. The domain spacing is more sensitive to changes in temperature and PE–PP volume fraction than the correlation length.

The temperatures of the lamellae to microemulsion transition in B20 and B15 were obtained by studying the second-order SANS peak at  $q = q_2$ . The SANS profiles in the vicinity of the second-order peak ( $0.1$ – $0.17$  nm<sup>-1</sup> for B20 and  $0.08$ – $0.14$  nm<sup>-1</sup> for B15) were assumed to be Gaussian functions of  $q$ :

$$I(q) = C \exp[-(q - q_2)^2/\sigma^2] + I_{bgd}(q) \quad (4)$$

where  $1/I_{bgd}(q)$  was assumed to be a quadratic function of  $q$ . In Figure 5 we show typical temperature dependence of the area under the second-order peak,  $I_2 = \pi^{1/2} C \sigma$ . For the B20 sample discussed in Figure 5, the

second-order peak intensity becomes small at 160 °C. This indicates that the lamellae-to-microemulsion transition temperature, as determined by SANS, is  $160 \pm 5$  °C. Similar analysis was conducted on the SANS profiles obtained from B15, identifying the lamellae-to-microemulsion transition temperature of  $150 \pm 5$  °C. The lamellae-to-microemulsion transition in B30 could not be studied by SANS due to the absence of a second-order peak in the accessible  $q$ -window.

The microemulsion-to-macrophase separation transition was identified by studying the SANS intensity at low  $q$  (see Figure 4a,b). The absence of a scattering peak and significant forward scattering (194 °C for B20 and 179 °C for B15) were taken as a signature of macrophase separation. The microemulsion-to-macrophase separation transition temperatures, based on the midpoint of the temperature step taken at which phase separation was observed, of B20 and B15 are  $175 \pm 5$  and  $187 \pm 7$  °C. B30 did not show any evidence of a microemulsion-to-macrophase separation transition in the accessible temperature range.

Light scattering experiments were used to confirm the location of some of the phase transitions identified by SANS. Based on arguments given in the Introduction, the temperature at which we are most likely to obtain single-phase systems is  $T \approx T_b \approx 155$  °C. At 155 °C, B20 and B30 with 1 mm thick path lengths were optically clear when observed using the naked eye. In contrast, B10 and B15 were turbid at 155 °C. The interpretation of light scattering experiments from turbid systems is not straightforward due to complications arising from multiple scattering. We thus only discuss light scattering data obtained from samples B20 and B30.

The  $I_{SALS}$  signal from pure block copolymers in both lamellar and disordered states is negligibly small. On the other hand, the transition from a lamellar phase to disorder in pure block copolymers is accompanied by a sharp decrease in  $I_{DSALS}$  to zero.<sup>68,69</sup> The  $I_{DSALS}$  signal in lamellar block copolymers arises due to the long-range coherent order, i.e., the presence of lamellar grains in the sample. In simple binary fluids, the formation of macroscopic phases is accompanied by a large increase in  $I_{SALS}$ .<sup>70</sup> Thus, lamellar phases are characterized by large  $I_{DSALS}$  and small  $I_{SALS}$  signals, while macrophase-separated samples are characterized by large  $I_{SALS}$  signals. Microemulsions have neither long-range order nor macroscopic phases, and they are thus characterized by small  $I_{DSALS}$  and small  $I_{SALS}$  signals. Now consider the upper half of the tail of the fish phase diagram shown in Figure 2. We expect large  $I_{DSALS}$  and small  $I_{SALS}$  at  $T \approx T_b$  (lamellar phase). Increasing the temperature to obtain the microemulsion phase will result in a decrease in  $I_{DSALS}$  to zero while maintaining negligible  $I_{SALS}$  signals. Further increase in temperature to obtain macrophase separation will result in an increase in the  $I_{SALS}$  signal.

In Figure 6, we show the results of light scattering experiments on the B30 blend. The time dependence of  $I_{SALS}$  was monitored after subjecting it to a series of step increases in temperature, starting from 140 °C. The sample was equilibrated for about 30 min at each temperature before subjecting it to the next step.  $I_{SALS}$  was extremely small (0.035 units) at temperatures below 195 °C. An example of this is shown in Figure 6a where we show the results of the 185 to 195 °C step. The next step from 195 to 204 °C resulted in a

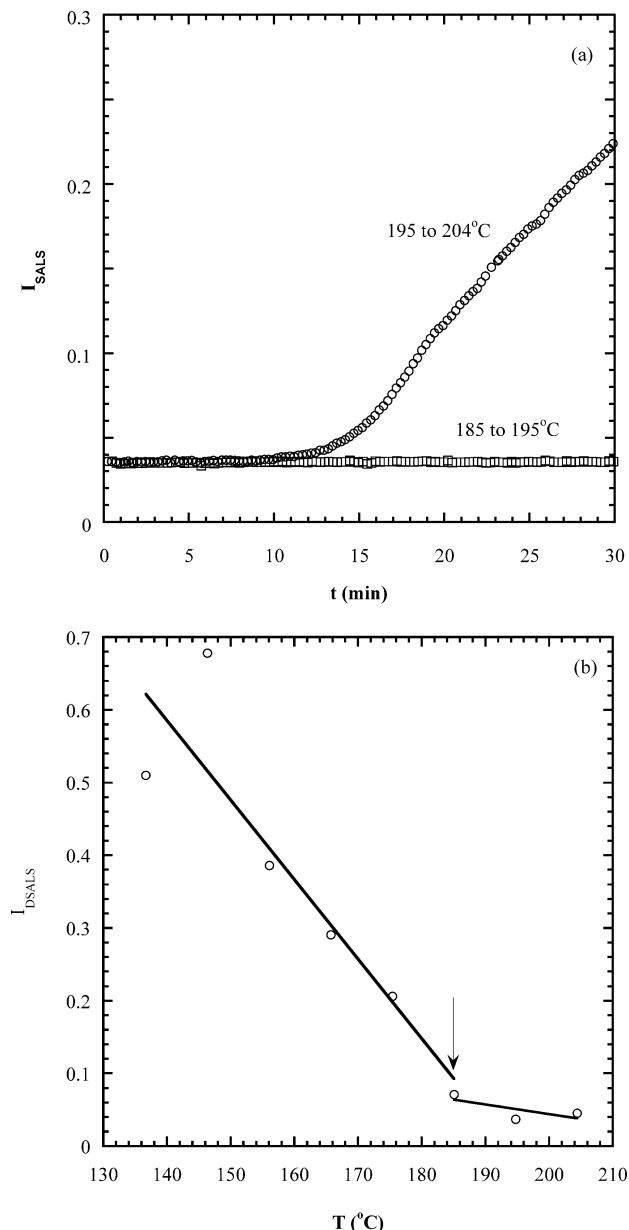


**Figure 6.** Results of light scattering experiments on B30. (a) Time dependence of the small-angle light scattering intensity  $I_{SALS}$  after step changes in temperature as indicated. The monotonic increase in  $I_{SALS}$  with time after the 195–204 °C step indicates macrophase separation. (b) Temperature dependence of the depolarized light scattering intensity  $I_{DSALS}$ . The arrow at 185 °C indicates a transition from an ordered lamellar phase with finite  $I_{DSALS}$  to a disordered microemulsion phase with negligible  $I_{DSALS}$ . A two-line linear least-squares fit<sup>78</sup> was used to determine the transition temperature.

monotonic increase in  $I_{SALS}$ , as seen in Figure 6a. This is a classic signature of macrophase separation, and we conclude that B30 is macrophase-separated at temperatures above  $200 \pm 5$  °C.

DSALS experiments were conducted on B30 using the same thermal history as that used for the SALS experiments. At each temperature,  $I_{DSALS}$  reached a steady-state value (or nearly so) after 30 min of equilibration. The temperature dependence of the steady-state  $I_{DSALS}$  value thus obtained from B30 is shown in Figure 6b. At temperatures below 185 °C,  $I_{DSALS}$  is a rapidly decreasing function of temperature. At temperatures above 185 °C,  $I_{DSALS}$  is nearly zero and independent of temperature. On the basis of arguments given above,

we conclude that the lamellae, which give rise to the excess depolarized light scattering intensity at low temperatures, disappear at  $185 \pm 5$  °C. Note that both SALS and DSALS data are consistent with the formation of lamellae at temperatures less than 185 °C (large  $I_{DSALS}$  and small  $I_{SALS}$ ), microemulsions from 185 to 200 °C (small  $I_{SALS}$  and small  $I_{DSALS}$ ), and macrophase separation above 200 °C (large  $I_{SALS}$ ). The lamellae-to-microemulsion transition of B30 is near the edge of the temperature window of the SANS experiments, while the microemulsion-to-macrophase separation transition lies outside the temperature window of the SANS experiments. We were thus unable to study these transitions by SANS.

Sample B20 was subjected to SALS and DSALS experiments with the same protocol that was used to study B30. The time dependence of the  $I_{SALS}$  data, shown in Figure 7a, is qualitatively similar to those obtained from B30 (Figure 6a), indicating a macrophase separation transition at  $180 \pm 5$  °C. The temperature dependence of the steady-state  $I_{DSALS}$  value thus obtained from B20 is shown in Figure 6b. At temperatures below 153 °C,  $I_{DSALS}$  is a rapidly decreasing function of temperature. At temperatures above 153 °C,  $I_{DSALS}$  is nearly independent of temperature. On the basis of arguments given above, we conclude that the lamellae, which give rise to the excess depolarized light scattering intensity at low temperatures, disappear at  $153 \pm 5$  °C. The lamellae-to-microemulsion and microemulsion-to-macrophase separation transition temperatures for B20 determined by light scattering and neutron scattering (given above) are in excellent agreement.

There are two important differences in the light scattering data obtained from B20 and B30: (1) The magnitude of  $I_{SALS}$  from B20 at the quench prior to macrophase separation is about an order of magnitude larger than that obtained from B30 under similar conditions (compare Figures 6a and 7a). (2) The value of  $I_{DSALS}$  of B20 in the region where the lamellae are no longer present is substantially larger than that obtained from B30 (compare Figures 6b and 7b). These complications are, perhaps, not surprising when one acknowledges the fact that the lamellar phase of sample B15 causes multiple light scattering.<sup>40</sup> Thus, there is a systematic increase in the complexity of the optical properties of single-phase A/B/A–C blends as the A–C concentration is reduced. The interpretation of light scattering data from simple systems such as pure block copolymers is straightforward due to two simplifying features: (1) the size of block copolymer lamellae is much smaller than the wavelength of light so  $I_{SALS} \approx 0$ , and (2) the disordered phase is featureless, and thus  $I_{DSALS} \approx 0$  when disordered. While these simplifications appear to hold for B30, they do not hold for B20. The SANS data indicate that the characteristic lengths of the lamellar and microemulsion phases in B20 are about 100 nm, only a factor of 5–6 smaller than the wavelength of light. This fact combined with additional factors such as lamellar undulations is probably responsible for the “anomalous” light scattering signals observed in sample B20. Despite this, there is no ambiguity in locating the macrophase separation transition (Figure 7a) and the disordering of the lamellar phase (Figure 7b) of B20.

The phase diagram of our PE/PIB/PE–PP blends in  $T$ – $\phi_{PE-PP}$  space, along the  $\phi_{PE}/\phi_{PIB} = 1.05$  isopleth, based on SANS, SALS, and DSALS experiments, is

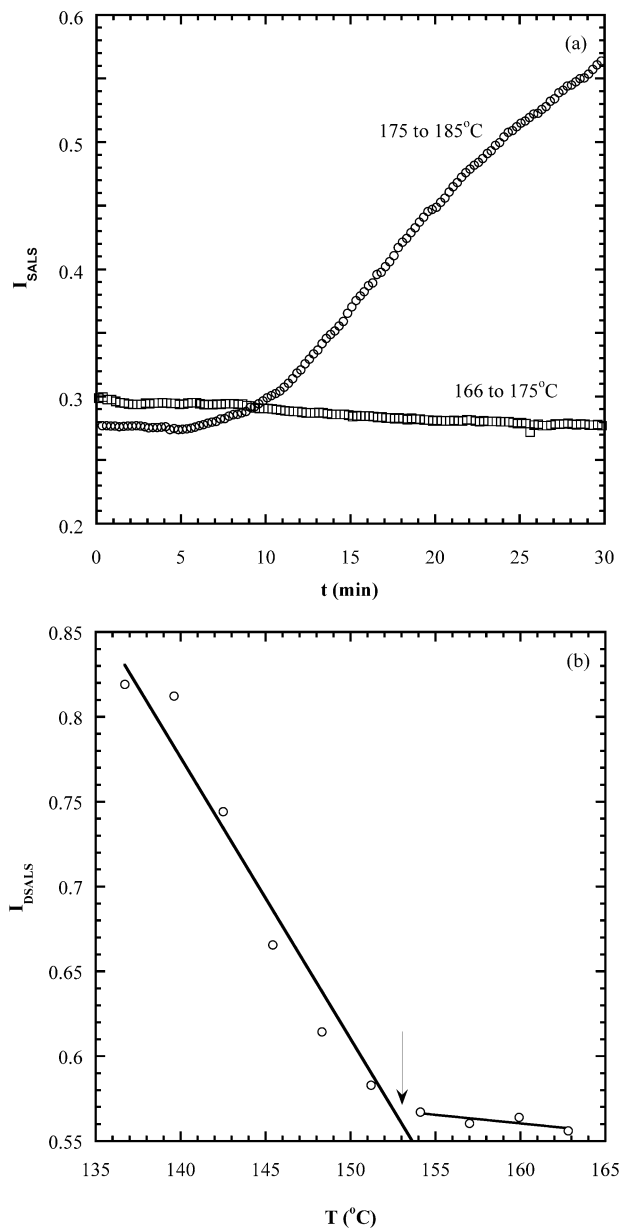


**Figure 7.** Results of light scattering experiments on B20. (a) Time dependence of the small-angle light scattering intensity  $I_{SALS}$  after step changes in temperature as indicated. The monotonic increase in  $I_{SALS}$  with time after the 175–185 °C step indicates macrophase separation. (b) Temperature dependence of the depolarized light scattering intensity  $I_{DSALS}$ . The arrow at 153 °C indicates a transition from an ordered lamellar phase to a disordered microemulsion phase. A two-line linear least-squares fit<sup>78</sup> was used to determine the transition temperature.

shown in Figure 8a. We were able to distinguish between lamellar phases (L), microemulsions (M), and phase-separated systems (2P). The phase diagram for PE/PIB/PE–PP blends shows a strong resemblance to the upper half of the oil/water/balanced surfactant fish phase diagram shown in Figure 2. It is clear, however, that our system is complex, and additional characterization of the phase transitions observed in reciprocal space is necessary. We thus conducted TEM experiments on samples located near the edge of the tail of the fish. This region of the phase diagram is expanded in Figure 8b. The symbols in Figure 8b indicate the locations of the samples studied by TEM on the phase diagram. The

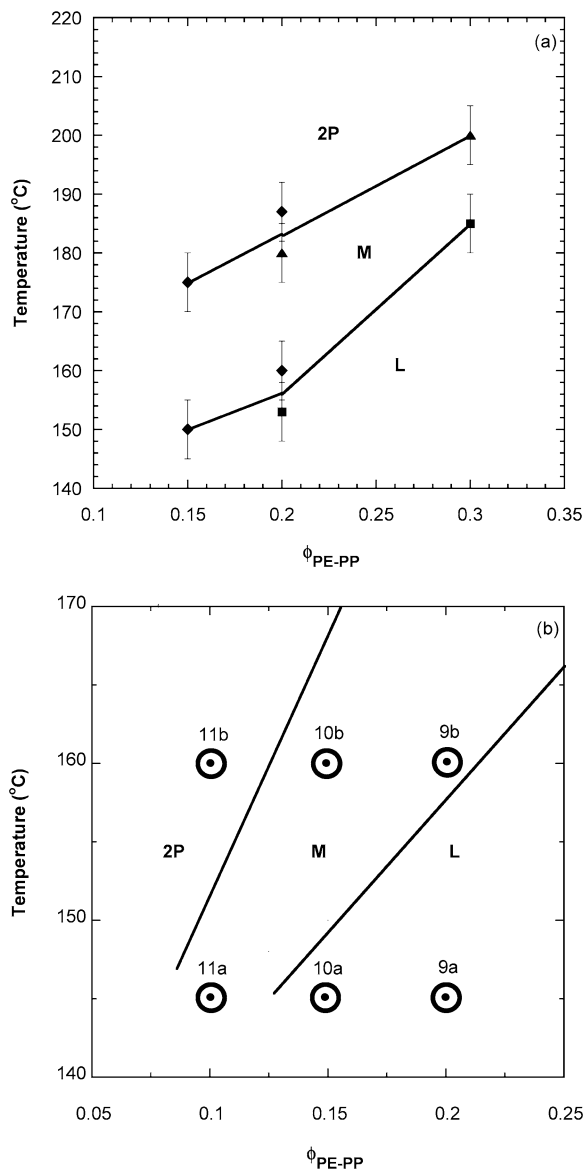


**Figure 8.** Phase diagram of PE/PIB/PE–PP blends along the  $\phi_{PE}/\phi_{PIB} = 1.05$  isopleth in  $T$ – $\phi_{PE-PP}$  space ( $\phi_i$  is the volume fraction of component  $i$ ). L denotes the lamellar phase, M denotes the microemulsion phase, and 2P denotes the two-phase region. (a) The transition temperatures were identified by SANS (diamonds), SALS (triangles), and depolarized SALS (squares). (b) Experimental phase diagram near the tail of the fish. The diblock concentration and temperature of the TEM samples are indicated by a dot, labeled with the corresponding figure number where the TEM result is shown. The lines represent results of TEM, SANS, USANS, SALS, and DSALS.

**Table 3. Summary of SANS Results for TEM Images**

|     | phase at 145 °C ( $d$ , nm) | phase at 160 °C ( $d$ , nm) |
|-----|-----------------------------|-----------------------------|
| B10 | unresolved                  | phase separated             |
| B15 | lamellar (120)              | microemulsion (155)         |
| B20 | lamellar (90)               | microemulsion (95)          |

SANS results obtained from these samples are summarized in Table 3.

In Figure 9a we show a TEM micrograph obtained from B20 at 145 °C, indicating clear evidence of a lamellar phase. We see thin dark lamellae separating broad bright lamellae. The average distance between adjacent dark (or bright) lamellae is about 54 nm. We obtained several micrographs from B20 at 145 °C and found that the distance between adjacent dark bands

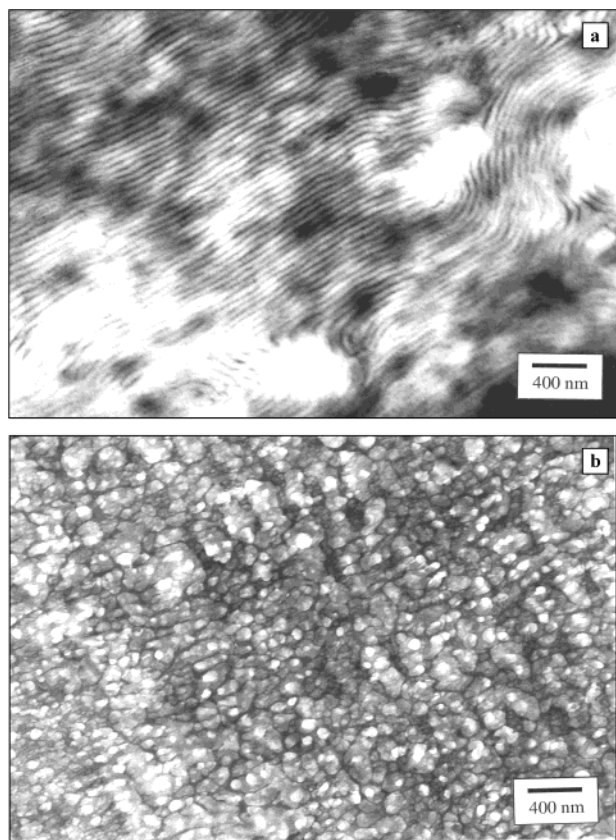


**Figure 9.** Transmission electron micrographs of the (a) lamellar ( $T = 145\text{ }^{\circ}\text{C}$ ) and (b) droplet microemulsion ( $T = 160\text{ }^{\circ}\text{C}$ ) phases of sample B20.

varied between 45 and 55 nm. The center-to-center distance between adjacent PIB (or PE) lamellae,  $d$ , of B20, obtained from SANS, was 90 nm (Table 3). The spacing between lamellae seen with TEM ( $d_{\text{TEM}}$ ) is thus expected to be 90 nm or larger.<sup>71</sup> The apparent discrepancy between the TEM and SANS data is resolved by recognizing that the PP-block of the copolymer is the most heavily stained component. Sample B20 contains 40% (by volume) of PE, 40% PIB, and 20% PE-PP. The apparent volume fraction occupied by the dark lamellae in Figure 9a is roughly consistent with the volume fraction of the PP-block. The dark bands in Figure 9a thus represent the location of the block copolymer, and the bright broader bands represent alternating layers of PE and PIB. We have no explanation for the lack of appreciable staining contrast between the PE and PIB lamellae. The characteristic period of the lamellar phase is thus twice the distance between dark lamellae. Using the smallest distance seen in the TEM micrographs, we obtain an estimate of 90–100 nm for the lamellar spacing, which is in excellent agreement with the SANS results.

In Figure 9b we show a micrograph obtained after annealing B20 at 160 °C. It is clear that heating the sample from 145 to 160 °C results in a dramatic change in morphology: the lamellar phase gives way to a fine dispersion of nearly monodisperse droplets. On the basis of arguments given in the Experimental Section, we expect the brightest phase to be PIB. We thus conclude that the droplets in Figure 9b are composed of PIB. This is consistent with arguments given in the Introduction that in an A/B/A-C blend one expects the formation of B droplets at high temperature (see Table 1). In oil/water systems, the high-temperature microemulsion

phase is known to comprise water droplets.<sup>34</sup> In addition, the characteristic length scale of the microemulsion, determined by SANS to be 95 nm (Table 3), is in agreement with the average intersphere distance seen in Figure 9b.

It is evident that images of B20 (Figure 9a,b) are in quantitative agreement with the SANS data (Table 3) and with the expected fish phase diagram (Figures 2 and 8). It is not possible to distinguish between droplet microemulsions and bicontinuous microemulsions on the basis of SANS because both systems give scattering curves that are in approximate agreement with the Teubner-Strey scattering profile.<sup>39</sup> Similarly, our light scattering analysis was incapable of distinguishing between droplet and bicontinuous microemulsions. The TEM data presented here thus provides the first evidence of the presence of a single droplet microemulsion phase. To our knowledge, this type of microemulsion has not been previously observed in polymeric systems. While the agreement between SANS and TEM is encouraging, the extent to which the TEM data represent the true structure of the PE/PIB/PE-PP mixtures at elevated temperatures is not clear. If the droplet microemulsion in Figure 9b were in perfect agreement with expectation, then the spheres would be in a grayish background (PE) and coated with a dark band representing the PE-PP block copolymer. However, what we see in Figure 9b is a dark network in a gray background. It is conceivable that this is due to the finite time taken to quench the sample from 160 °C. While cooling, the sample spends a finite amount of time in the lamellar region of the phase diagram, and it is conceivable that some rearrangement of the molecules has taken place. Since the surfactant layer is only one molecule thick, it rearranges more rapidly than the droplets because each droplet contains about  $10^4$  polymer molecules. While a detailed interpretation of all aspects of the position space images obtained from the droplet microemulsions is not yet possible, the TEM data clearly indicate the presence of PIB droplets at 160 °C.

In parts a and b of Figure 10, we show typical micrographs obtained from sample B15 at 145 and 160 °C, respectively. The data obtained from B15 and B20 are qualitatively similar. At 145 °C, we see a lamellar phase (Figure 10a). There are, however, two quantitative differences between the lamellae formed in B15 and B20: (1) The characteristic repeat distance is significantly larger in B15 than that seen in B20, and (2) the lamellae are much less ordered in B15 than B20. Both facts are consistent with the SANS data:  $q_{\text{peak}}$  of B15 is smaller than that of B20, and the peak width obtained in B15 is larger than that of B20. Heating B15 to 160 °C results in a transformation from lamellae to spheres, as expected from the phase diagram shown in Figure 8. The spheres obtained in B15 are larger in diameter on average than those obtained in B20, and the average intersphere distance is correspondingly larger.

Having established the presence of the single droplet microemulsion phase in B15 and B20, we return briefly to the SANS data obtained from these samples. Microemulsions are usually characterized by a single scattering peak. In our microemulsions, however, there is a hint of a broad secondary peak in the microemulsion phase: refer to the 160 and 179 °C data in Figure 4a as well as the 160 °C data in Figure 4b. The radii of the droplets formed at 160 °C in our samples,  $R$ , are about 50 nm in B20 (Figure 9b) and about 100 nm in B15

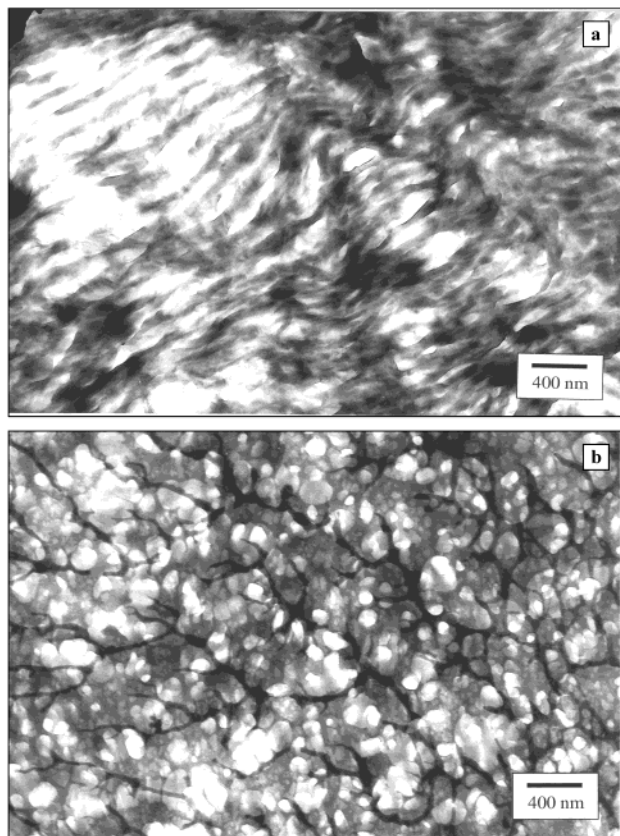


**Figure 10.** Transmission electron micrographs of the (a) lamellar ( $T = 145\text{ }^{\circ}\text{C}$ ) and (b) droplet microemulsion ( $T = 160\text{ }^{\circ}\text{C}$ ) phases of sample B15.

(Figure 10b). The form factor of spheres has a maximum at  $qR = 5.7$ . We would thus expect weak scattering maxima at  $q \approx 0.11\text{ nm}^{-1}$  in the B20 SANS profile at  $160\text{ }^{\circ}\text{C}$  and at  $q \approx 0.06\text{ nm}^{-1}$  in B15 SANS profile at  $160\text{ }^{\circ}\text{C}$ . It is thus evident that the broad secondary scattering peaks seen in the microemulsion phase in samples B15 and B20 (the  $160\text{ }^{\circ}\text{C}$  data in Figure 4a,b) are due to the presence of PIB droplets.<sup>72</sup>

We now return to the TEM data obtained from our samples. In Figure 11a we show a TEM micrograph obtained from sample B10 at  $145\text{ }^{\circ}\text{C}$ . The structure observed is very similar to that obtained from bicontinuous oil/water microemulsions.<sup>34</sup> We see white PIB-rich regions interspersed in gray PE-rich regions. Images of bicontinuous microemulsions are difficult to obtain, and in our opinion, the best example of one is given in ref 6. While Figure 11a is not as clear as that given in ref 6, it compares favorably to other images of bicontinuous microemulsions in the literature.<sup>73,74</sup> We observe a broad distribution of distances between adjacent PIB-rich domains with an average of about  $500\text{ nm}$ .<sup>75</sup> The scattering peak from such a structure would be extremely broad and would appear near the low- $q$  limit of the SANS detector. The large structures seen in the TEM may also lead to multiple scattering, which would lead to further broadening of the scattering peak. Heating B10 to  $160\text{ }^{\circ}\text{C}$  results in a macrophase-separated state with no evidence of periodicity, as shown in Figure 11b. Note, however, that the size of the macrophase-separated domains is no larger than  $800\text{ nm}$ , although the sample was annealed in the two-phase region for 2 h. It is clear that the proximity of the blend to the single-phase tail of the fish phase diagram leads to extremely slow phase separation kinetics.

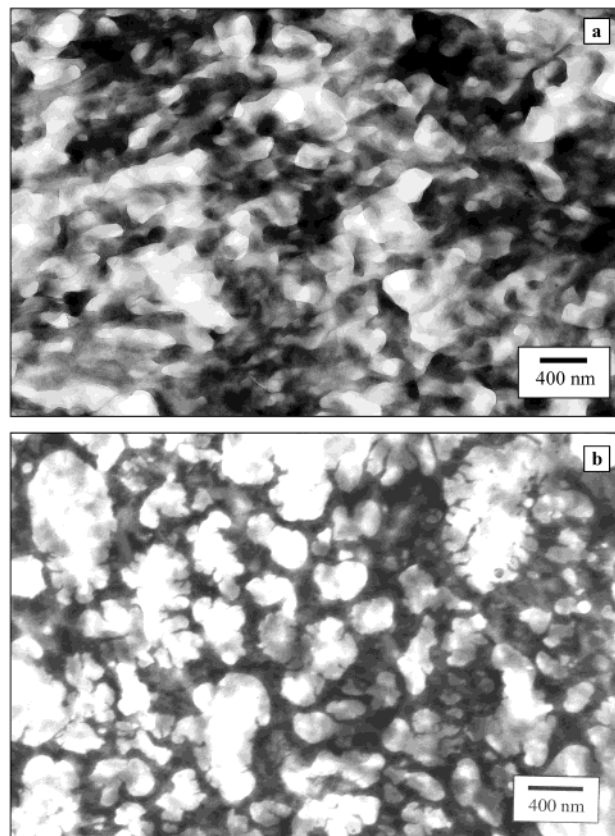


**Figure 11.** Transmission electron micrographs of the (a) bicontinuous microemulsion ( $T = 145\text{ }^{\circ}\text{C}$ ) and (b) macrophase separated ( $T = 160\text{ }^{\circ}\text{C}$ ) states of sample B10.

Upon completion of the SANS and TEM experiments it became clear that further study of sample B10 at  $145\text{ }^{\circ}\text{C}$  was necessary to confirm our conclusion regarding its structure. We thus conducted USANS experiments on B10 at a mean temperature of  $143\text{ }^{\circ}\text{C}$ . We chose a slightly lower temperature for the USANS experiments because the temperature control of the oven used to house the sample was not working perfectly at the time of our experiment. It took about 24 h to measure each scattering profile, and over this time we observed drifts in the sample temperature that were as high as  $\pm 2\text{ }^{\circ}\text{C}$ . Since the TEM results indicated a transition from a microemulsion to macrophase separation between  $145$  and  $160\text{ }^{\circ}\text{C}$ , we decided on a mean sample temperature of  $143\text{ }^{\circ}\text{C}$  to ensure that our sample did not enter the phase-separated region of the phase diagram during the experiment. The measured scattering profile from B10 at  $143 \pm 2\text{ }^{\circ}\text{C}$  is shown in Figure 12. We find a broad but noticeable shoulder in the USANS profile in the vicinity of  $q = 0.01\text{ nm}^{-1}$ . This shoulder appears to be superposed on a  $q^{-3}$  background. Note that similar background scattering was seen in the SANS data from samples B15 and B20 (dashed curves in Figures 4a,b). Also shown in Figure 12 are the low- $q$  SANS data obtained from B10 at  $145\text{ }^{\circ}\text{C}$ . The absolute SANS and USANS data presented in Figure 12 are shown with no adjustable parameters. In theory, the SANS and USANS data sets should be continuous. The observed offset is probably due to the thickness difference between the two samples. (The USANS sample thickness was reduced to avoid multiple scattering.) We repeated the USANS measurements on B10 two times to confirm the presence of the scattering shoulder shown in Figure 12. The USANS (and SANS) data in Figure 12 provide some

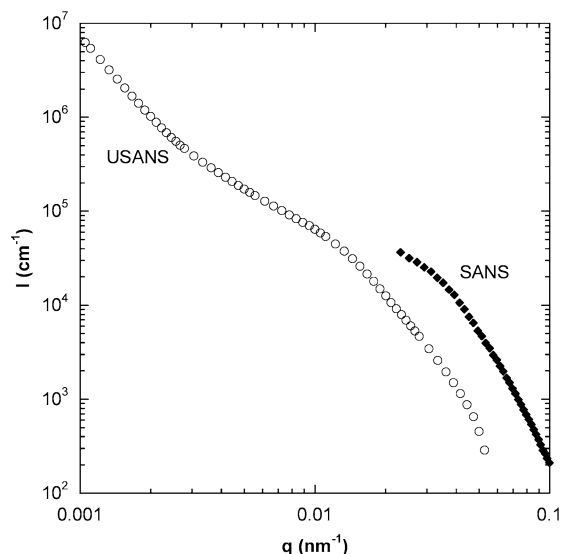


**Figure 12.** Both SANS and USANS data are shown for B10 (10% PE-PP).<sup>77</sup> The SANS data were taken at  $145 \pm 1$  °C, and the USANS data were taken at  $143 \pm 2$  °C.

support to our conclusion regarding the state of B10 at 145 °C based on TEM.

The micrographs in Figures 9–11 confirm the existence of the three phase transitions indicated by the arrows in Figure 2. Figures 9 and 10 confirm the lamellae-to-spherical microemulsion transition indicated by arrow A in Figure 2. A comparison of Figures 9a, 10a, and 11a confirms the lamellae-to-bicontinuous microemulsion transition indicated by arrow B in Figure 2. Figure 11 confirms the bicontinuous microemulsion-to-phase-separated structure transition, indicated by arrow C in Figure 2. A combination of experiments—SANS, USANS, SALS, DSALS, and TEM—was necessary to determine the location of the phase transitions, indicated by lines in Figure 8a,b.<sup>76</sup> It is clear from a comparison of Figures 8b and 2 that the balance temperature  $T_b$  of our PE/PIB/PE-PP system is below but close to 145 °C. This is in reasonable agreement with our initial estimate of 155 °C (see Introduction), which was based entirely on the temperature dependence of  $\chi_{PP/PIB}$  obtained from binary blends.<sup>43</sup>

### Concluding Remarks

The nature of phase transitions in mixtures of highly immiscible PE/PIB polymers stabilized by a PE-PP diblock copolymer was studied by a combination of experiments in both position and reciprocal space. The phase diagram along the isopleth when the PE-PP surfactant is added to a 50/50 PE/PIB mixture has the shape of a fish, as shown in Figures 2 and 9. TEM and SANS data provide clear evidence for a variety of interesting phase transitions. At 145 °C, we find a transition from lamellae to a bicontinuous microemulsion as  $\phi_{A-C}$  is reduced from 0.15 to 0.10. A similar transition is seen in the A/B/A-B blends studied by Bates, Lodge, and co-workers.<sup>6</sup> The main difference is that the A/B polymers used in ref 6 were nearly miscible ( $\chi_{AB}N \approx 2$ ). In contrast, in our system  $\chi_{AB}N$  is significantly larger than 2. We also demonstrated that heating the bicontinuous microemulsion leads to macrophase separation, while heating the lamellar phase leads to the formation of a single droplet microemulsion phase. To our knowledge, these phase transitions have only been observed in aqueous mixtures. In A/B/A-B sys-

tems, for example, one obtains two macrophases of coexisting droplet microemulsions.<sup>4-7</sup>

It is clear that immiscible fluids A and B, either aqueous or polymeric, can be stabilized by an A-C surfactant provided that the C-block is chosen in a manner that balances the attractive and repulsive interactions between the surfactant and the A-rich and B-rich phases. Our work demonstrates that surfactant design in generalized A/B mixtures requires control over four independent characteristics of the surfactant: A-philicity, A-phobicity, B-philicity, and B-phobicity. In mixtures such as polyolefins, these characteristics are related to the Flory-Huggins interaction parameters between the components and perhaps other parameters such as the statistical segment lengths. To our knowledge, our work represents the first application of the surfactant design principles, proposed by Khalweit and co-workers for aqueous mixtures, to mixtures wherein dipole-dipole and hydrogen-bonding interactions are absent. We hope that this work will provide the motivation for future theories and experiments that go beyond the traditional approach of using A-B copolymers to stabilize A/B blends.

**Acknowledgment.** This paper was strengthened by the critical comments and suggestions of the referees and the editor. Educational discussions with Ben Reynolds are acknowledged. The work at the University of California, Berkeley, was supported by the National Science Foundation under Grant CTS-0201211. The work at the University of Massachusetts, Amherst, was supported by the US Army Research Office under Grant DAAD19-01-1-0544. The facilities at NIST are supported in part by the National Science Foundation under Agreement DMR-9986442.<sup>79</sup>

### References and Notes

- (1) Safran, S. *Statistical Thermodynamics of Surfaces, Interfaces, and Membranes*; Addison-Wesley: Reading, MA, 1994.
- (2) Israelachvili, J. *Intermolecular and Surface Forces*; Academic Press: London, 1997.
- (3) Davis, H. T. *Statistical Mechanics of Phases, Interfaces, and Thin Films*; Wiley-VCH: New York, 1996.
- (4) Bates, F. S.; Maurer, W. W.; Lodge, T. P.; Schulz, M. F.; Matsen, M. W. *Phys. Rev. Lett.* **1995**, *75*, 4429.
- (5) Hillmyer, M. A.; Maurer, W. W.; Lodge, T. P.; Bates, F. S.; Almdal, K. *J. Phys. Chem. B* **1999**, *103*, 4814.
- (6) Bates, F. S.; Maurer, W. W.; Lipic, P. M.; Hillmyer, M. A.; Almdal, K.; Mortensen, K.; Fredrickson, G. H.; Lodge, T. P. *Phys. Rev. Lett.* **1997**, *79*, 849.
- (7) Washburn, N. R.; Lodge, T. P.; Bates, F. S. *J. Phys. Chem. B* **2000**, *104*, 6987.
- (8) Morkved, T. L.; Chapman, B. R.; Bates, F. S.; Lodge, T. P.; Stepanek, P.; Almdal, K. *Faraday Discuss.* **1999**, *112*, 335.
- (9) Cohen, R. E.; Ramos, A. R. *Macromolecules* **1979**, *12*, 131.
- (10) Dutta, S.; Lohse, D. J. *Polymeric Compatibilizers*; Hanser: Cincinnati, OH, 1996.
- (11) Hudson, S. D.; Jamieson, A. M. In *Polymer Blends*; Paul, C. B., Ed.; Wiley: New York, 2000; Vol. 1, p 461.
- (12) Jeon, H. S.; Lee, J. H.; Balsara, N. P. *Phys. Rev. Lett.* **1997**, *79*, 3274.
- (13) Jeon, H. S.; Lee, J. H.; Balsara, N. P. *Macromolecules* **1998**, *31*, 3328.
- (14) Jeon, H. S.; Lee, J. H.; Balsara, N. P.; Newstein, M. C. *Macromolecules* **1998**, *31*, 3340.
- (15) Lyu, S.; Jones, T. D.; Bates, F. S.; Macosko, C. W. *Macromolecules* **2002**, *35*, 7845.
- (16) Beck Tan, N. C.; Tai, S. K.; Briber, R. M. *Polymer* **1996**, *37*, 3509.
- (17) Jackson, C. L.; Sung, L.; Han, C. C. *Polym. Eng. Sci.* **1997**, *37*, 1449.
- (18) Sung, L.; Hess, D. B.; Jackson, C. L.; Han, C. C. *J. Polym. Res. (Taiwan)* **1996**, *3*, 139.

- (19) Koizumi, S.; Hasegawa, H.; Hashimoto, T. *Macromolecules* **1994**, *27*, 7893.
- (20) Kielhorn, L.; Muthukumar, M. *J. Chem. Phys.* **1997**, *107*, 5588.
- (21) Balsara, N. P.; Jonnalagadda, S. V.; Lin, C. C.; Han, C. C.; Krishnamoorti, R. *J. Chem. Phys.* **1993**, *99*, 10011.
- (22) Leibler, L. *Physica A* **1991**, *172*, 258.
- (23) Leibler, L. *Makromol. Chem. Macromol. Symp.* **1988**, *16*, 1.
- (24) Broseta, D.; Fredrickson, G. H. *J. Chem. Phys.* **1990**, *93*, 2927.
- (25) Mathur, D.; Hariharan, R.; Neuman, E. B. *Polymer* **1999**, *40*, 6077.
- (26) Wang, Z. G.; Safran, S. A. *J. Phys. (Paris)* **1990**, *51*, 185.
- (27) Janert, P. K.; Schick, M. *Macromolecules* **1997**, *30*, 137.
- (28) Janert, P. K.; Schick, M. *Macromolecules* **1997**, *30*, 3916.
- (29) Müller, M.; Schick, S. *J. Chem. Phys.* **1996**, *105*, 8885.
- (30) Maric, M.; Macosko, C. W. *J. Polym. Sci., Polym. Phys.* **2002**, *40*, 346.
- (31) Schnell, R.; Stamm, M.; Rauch, F. *Macromol. Chem. Phys.* **1999**, *200*, 1806.
- (32) Zhao, H. Y.; Huang, B. T. *J. Polym. Sci., Polym. Phys.* **1998**, *36*, 85.
- (33) Kahlweit, M.; Strey, R. *Angew. Chem., Int. Ed. Engl.* **1985**, *24*, 654.
- (34) Strey, R. *Colloid Polym. Sci.* **1994**, *272*, 1005.
- (35) Chen, S. H.; Choi, S. *Supramol. Sci.* **1998**, *5*, 197.
- (36) Kahlweit, M.; Strey, R.; Firman, P.; Haase, D. *Langmuir* **1985**, *1*, 281.
- (37) Kahlweit, M.; Strey, R.; Haase, D.; Firman, P. *Langmuir* **1988**, *4*, 785.
- (38) Magid, L.; Butler, P.; Payne, K.; Strey, R. *J. Appl. Crystallogr.* **1988**, *21*, 832.
- (39) Teubner, M.; Strey, R. *J. Chem. Phys.* **1987**, *87*, 3195.
- (40) Lee, J. H.; Balsara, N. P.; Krishnamoorti, R.; Jeon, H. S.; Hammouda, B. *Macromolecules* **2001**, *34*, 6557.
- (41) The schematic in Figure 2 is only an approximate schematic. In real systems, the phase diagrams are not perfectly symmetric about  $T_b$ .<sup>33</sup>
- (42) Lee, J. H.; Balsara, N. P.; Chakraborty, A. K.; Krishnamoorti, R.; Hammouda, B. *Macromolecules* **2002**, *35*, 7748.
- (43) Krishnamoorti, R.; Graessley, W. W.; Fetters, L. J.; Garner, R. T.; Lohse, D. J. *Macromolecules* **1995**, *28*, 1252.
- (44) Balsara, N. P. *Physical Properties of Polymers Handbook*; AIP Press: New York, 1996; Chapter 19.
- (45) All of the PE/PIB blends made in our lab thus far have been phase-separated. It may be possible to obtain the  $\gamma$  parameter in this system by studying interfaces between thin films as was done in: Schubert, D. W. *Macromol. Symp.* **2000**, *149*, 257.
- (46) In some instances the block copolymer forms its own phase rather than exist at the interface between the two homopolymers.<sup>23,24,27,28</sup> For the purposes of this analysis, we will focus on the situation in which it is thermodynamically favorable for the block copolymer to exist at the interface.
- (47) Shull, K. *J. Chem. Phys.* **1991**, *94*, 5723.
- (48) Wang, Z. G. *Macromolecules* **1992**, *25*, 3702.
- (49) Adedeji, A.; Lyu, S.; Macosko, C. W. *Macromolecules* **2001**, *34*, 8663.
- (50) Adedeji, A.; Jamieson, A. M.; Hudson, S. D. *Macromolecules* **1995**, *28*, 5255.
- (51) Iizuka, N.; Bodycomb, J.; Hasegawa, H.; Hashimoto, T. *Macromolecules* **1998**, *31*, 7256.
- (52) Hashimoto, T.; Kimishima, K.; Hasegawa, H. *Macromolecules* **1991**, *24*, 5704.
- (53) Koizumi, S.; Hasegawa, H.; Hashimoto, T. *Makromol. Chem. Macromol. Symp.* **1992**, *62*, 75.
- (54) Hashimoto, T. *Macromol. Symp.* **1995**, *98*, 925.
- (55) Löwerhaupt, B.; Steurer, A.; Hellmann, G. P. *Macromolecules* **1994**, *27*, 908.
- (56) Storey, R. F.; Chisholm, B. J.; Brister, L. B. *Macromolecules* **1995**, *28*, 4055.
- (57) Lee, J. H. PhD Thesis, University of California, Berkeley, CA, 2002.
- (58) Tenaglia, A.; Terranova, E.; Waegell, B. *J. Org. Chem.* **1992**, *57*, 5523.
- (59) Khandpur, A. K.; Macosko, C. W.; Bates, F. S. *J. Polym. Sci., Part B* **1995**, *33*, 1527.
- (60) Dias, A. J. In *Polymeric Materials Encyclopedia*; Salamone, J., Ed.; CRC Press: New York, 1996; p 3484.
- (61) Previous studies have shown the relative inertness of PIB to OsO<sub>4</sub> staining.<sup>59</sup>
- (62) Storey, R. F.; Baugh, D. W. *Polymer* **2000**, *41*, 3205.
- (63) Kresge, E. N.; Schatz, R. H.; Wang, H. C. In *Encyclopedia of Polymer Science and Engineering*; Wiley & Sons: 1987; Vol. 18, p 423.
- (64) Cohen, R. E.; Cheng, P. L.; Douzinas, K.; Kofinas, P.; Berney, C. V. *Macromolecules* **1990**, *23*, 324.
- (65) Loo, Y. L.; Register, R. A.; Ryan, A. J.; Dee, G. T. *Macromolecules* **2001**, *34*, 8968.
- (66) Drews, A. R.; Barker, J. G.; Glinka, C. J.; Agamalian, M. *Physica B* **1998**, *241–243*, 189–191.
- (67) A quadratic function is adequate for fitting the measured scattering profiles in the neighborhood of the second-order peak.
- (68) Balsara, N. P.; Garetz, B. A.; Dai, H. J. *Macromolecules* **1992**, *25*, 6072.
- (69) Garetz, B. A.; Balsara, N. P.; Dai, H. J.; Wang, Z.; Newstein, M. C.; Majumdar, B. *Macromolecules* **1996**, *29*, 4675.
- (70) Balsara, N. P.; Fetters, L. J.; Hadjichristidis, N.; Lohse, D. J.; Han, C. C.; Graessley, W. W.; Krishnamoorti, R. *Macromolecules* **1992**, *25*, 6137.
- (71) The larger values would be obtained if the plane of the microtomed section were not orthogonal to the plane of the lamellae ( $d_{\text{TEM}} = d/\sin \theta$ , where  $\theta$  is the angle between the lamellar plane and the plane of the section). Slices through a collection of randomly oriented grains will be dominated by  $\theta = 90^\circ$ .
- (72) We thank one of the referees for suggesting this.
- (73) Kahlweit, M.; et al. *J. Colloid Interface Sci.* **1987**, *118*, 436.
- (74) Jahn, W.; Strey, R. In *Physics of Amphiphilic Layers, Proceedings in Physics*; Springer: Berlin, 1987; p 353.
- (75) An additional feature seen in many of the micrographs of B10 is the presence of very tiny black dots. This suggests the presence of micelles with PP cores. Whether these structures are present at 145 °C or they were formed during the TEM sample preparation remains an open question.
- (76) The coexistence window of lamellar and microemulsion phases is much narrower than the steps used to explore the phase behavior of our A/B/A–C blends.
- (77) The size of the error bars is comparable to the size of the symbols used to present the data.
- (78) Lefebvre, A. A.; Lee, J. H.; Balsara, N. P.; Vaidyanathan, C. *J. Chem. Phys.* **2002**, *117*, 9063.
- (79) Certain commercial equipment, instruments, or materials (or suppliers, software, etc.) are identified in this paper to foster understanding. Such identification does not imply recommendation or endorsement by the National Institute of Standards and Technology, nor does it imply that the materials or equipment identified are necessarily the best available for the purpose.

MA0340356